Eur. Phys. J. Special Topics **185**, 195–208 (2010)

DOI: 10.1140/epjst/e2010-01249-4

THE EUROPEAN PHYSICAL JOURNAL SPECIAL TOPICS

Regular Article

Rogue internal waves in the ocean: Long wave model

R. Grimshaw[1,a], E. Pelinovsky[2], T. Taipova[2], and A. Sergeeva[2]

[1] Loughborough University, UK
[2] Institute of Applied Physics, Nizhny Novogorod, Russia

Received in final form and accepted 15 June 2010
Published online 23 August 2010

Abstract. Rogue waves can be categorized as unexpectedly large waves, which are temporally and spatially localized. They have recently received much attention in the water wave context, and also been found in nonlinear optical fibers. In this paper, we examine the issue of whether rogue internal waves can be found in the ocean. Because large-amplitude internal waves are commonly observed in the coastal ocean, and are often modeled by weakly nonlinear long wave equations of the Korteweg-de Vries type, we focus our attention on this shallow-water context. Specifically, we examine the occurrence of rogue waves in the Gardner equation, which is an extended version of the Korteweg-de Vries equation with quadratic and cubic nonlinearity, and is commonly used for the modelling of internal solitary waves in the ocean. Importantly, we choose that version of the Gardner equation for which the coefficient of the cubic nonlinear term and the coefficient of the linear dispersive term have the same sign, as this allows for modulational instability. From numerical simulations of the evolution of a modulated narrow-band initial wave field, we identify several scenarios where rogue waves occur.

1 Introduction

The term rogue waves is commonly identified with unexpectedly large water waves in the ocean, which are spatially and temporally localized, see Kharif et al. (2009) for instance. Several mechanisms have been invoked including essentially linear processes such as directional focusing, or topographic and current focusing, and nonlinear processes such as modulational instability with the consequent nonlinear focusing of energy. Importantly the nonlinear processes are often based on appropriate solutions of the nonlinear Schrodinger equation (NLS) of the focusing kind, These, and other proposed mechanisms, can be realized in other physical systems, leading to the speculation that rogue waves can occur there as well. For instance, phenomena that can be categorized as rogue waves have recently been found in nonlinear optical fibers (Solli et al., 2007; Yeom et al., 2007; Akhmediev et al., 2009).

In this article, we examine the issue of whether rogue waves can occur for the case of internal waves in the ocean. In principle, all the physical mechanisms proposed for rogue water waves can be applied to internal waves. However, although very large amplitude internal waves have certainly been observed in the ocean, as far as we are aware their possible labeling as rogue waves has not been made. Internal waves in the ocean can be loosely categorized as either occurring in the deep ocean where they can propagate vertically, or occurring in the coastal ocean where they have a specific vertical structure and the emphasis is on their horizontal propagation. Here, we will examine the latter category. Huge internal waves in the ocean are often observed in the various parts of the coastal oceans. Their amplitudes can reach

[a] e-mail: R.H.J.Grimshaw@lboro.ac.uk

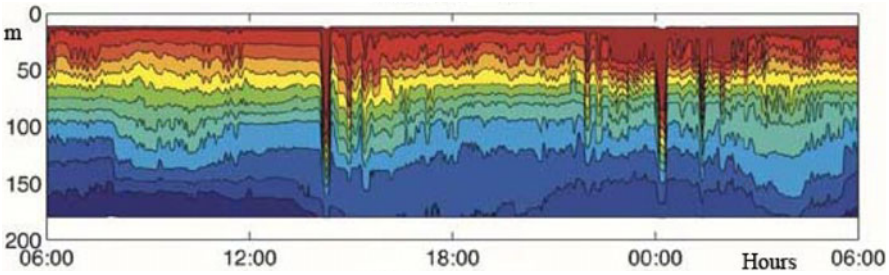

Fig. 1. Temperature time-series in the South China Sea (from Duda et al., 2004). The contour interval is 1 degree. The deepest blue color is the 15–16 degree range.

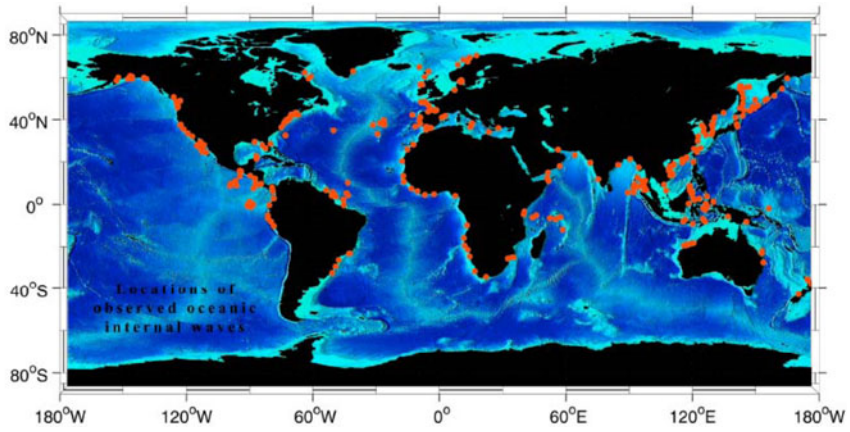

Fig. 2. Map showing sites where internal solitons have been reported, from `http://www.internalwaveatlas.com/`

50–100 meters (Orr and Mignerey, 2003; Duda et al., 2004; Apel et al., 2007). A typical example of solitary-like waves is demonstrated in Fig. 1 taken from Duda et al. (2004). The geographical distribution of similar observed large-amplitude internal waves is shown in Fig. 2 (Apel et al., 2007).

Physically, the existence of these large-amplitude internal waves is related to the enhanced effect of gravity due to the very small difference in density of neighbouring layers (of order 10^{-2}). These internal solitary-like waves are generated principally by the interaction of the barotropic tide with bottom topography, often the continental shelf; other mechanisms may include instability of ocean currents in zones with strong shear flow (such as an ocean gulf), or directly by wind stress. Usually, these large-amplitude internal solitary-like waves are modeled with nonlinear wave equations of the Korteweg-de Vries (KdV) type. These include the well-known integrable KdV equation, the same equation modified with variable coefficients and frictional terms, and extended equations which include higher order nonlinear terms, see the reviews by Grimshaw (2001) and Holloway et al. (2001) for instance. In this context the appearance of very large-amplitude waves is usually regarded as a deterministic process, where the large amplitudes are due to a combination of the initial conditions and the background density stratification.

However, this does not exclude the possibility that internal rogue waves can occur in some special circumstances. To explore this issue further requires a different approach, where it may be necessary to invoke statistical methods. For the case of water waves, the weak wave turbulence theory has been successfully used to model wave spectra. Analogous theories have been developed for deep ocean internal waves, see Muller and Olbers (1975), Olbers (1976), McComas (1977), Pelinovsky and Raevsky (1977), Caillol and Zeitlin (2001) and Lvov et al. (2004) for instance. But for the most part, these theories were developed for the deep ocean with an almost uniform density stratification, and hence are not relevant for application to internal waves

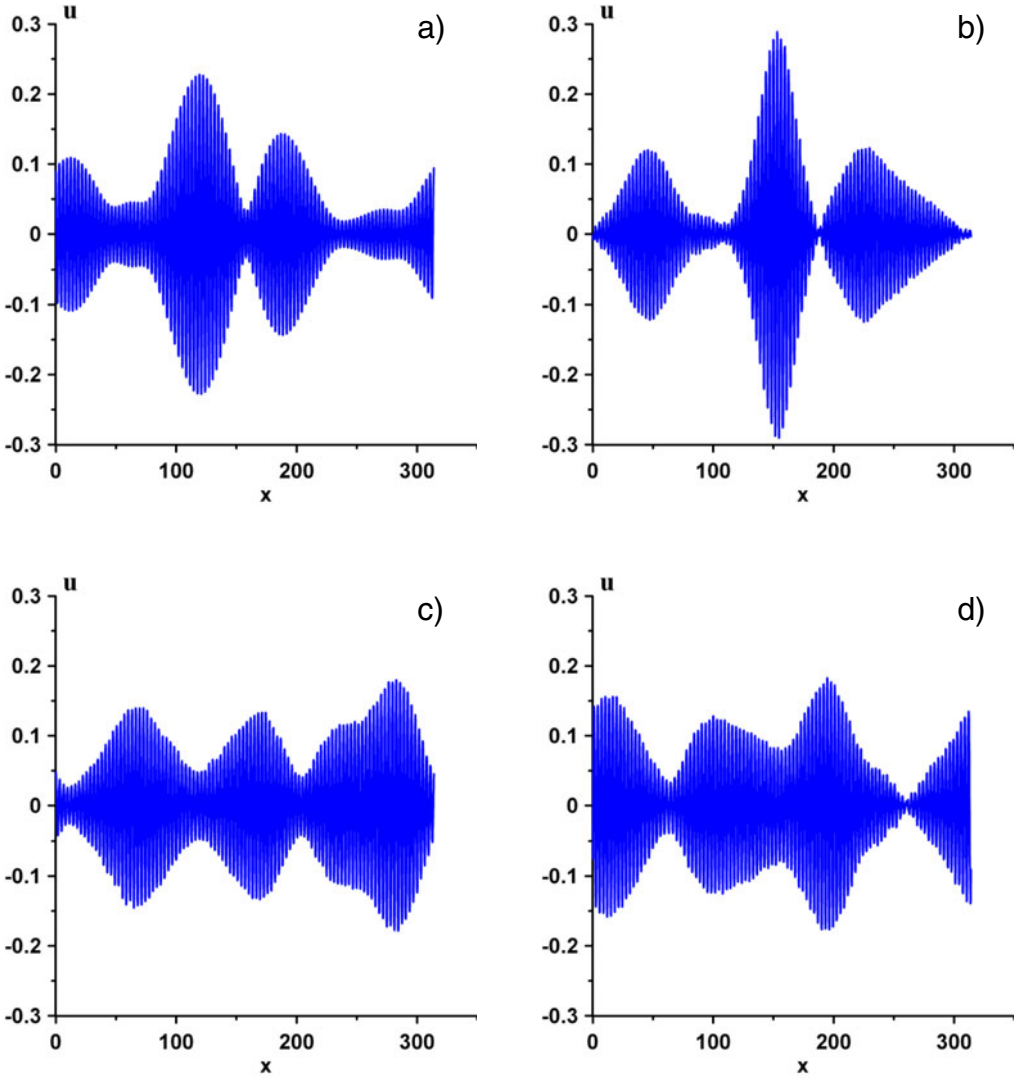

Fig. 3. Wave group evolution with initial amplitude 0.23, 6 satellites; (a) $t = 0$ top left, (b) $t = 50$ top right, (c) $t = 250$ bottom left, (d) $t = 500$ bottom right.

in the shallow coastal ocean. In this latter case, our concern is with the internal waves which ride on strong pycnoclines, and hence a modal approach is needed. In the simplest case of a two-layer model of the density stratification, the kinematic properties of linear interfacial waves are similar to the properties of the surface gravity waves, but there are significant differences in their nonlinear properties. In the more general case of a multi-layer or continuously stratified ocean, internal waves are described by many modes. We infer that the physical mechanisms for the formation of internal rogue waves may have some specific features when compared with surface rogue waves. Although a full statistical theory for internal waves in the coastal ocean is not available, a viable alternative is to use one of the model equations of the KdV-type, which are commonly used to study internal solitary waves. Thus, Pelinovsky and Sergeeva (2006) examined numerically the evolution of a random wave field in the KdV equation. It is well-known that the description of wave packets in the KdV equation by an asymptotic reduction to a NLS equation leads to the defocusing case and hence modulational stability. Hence the formation of rogue waves directly by modulational instability is not expected in the KdV model. However, Pelinovsky and Sergeeva (2006) found that the evolution of an initial Gaussian

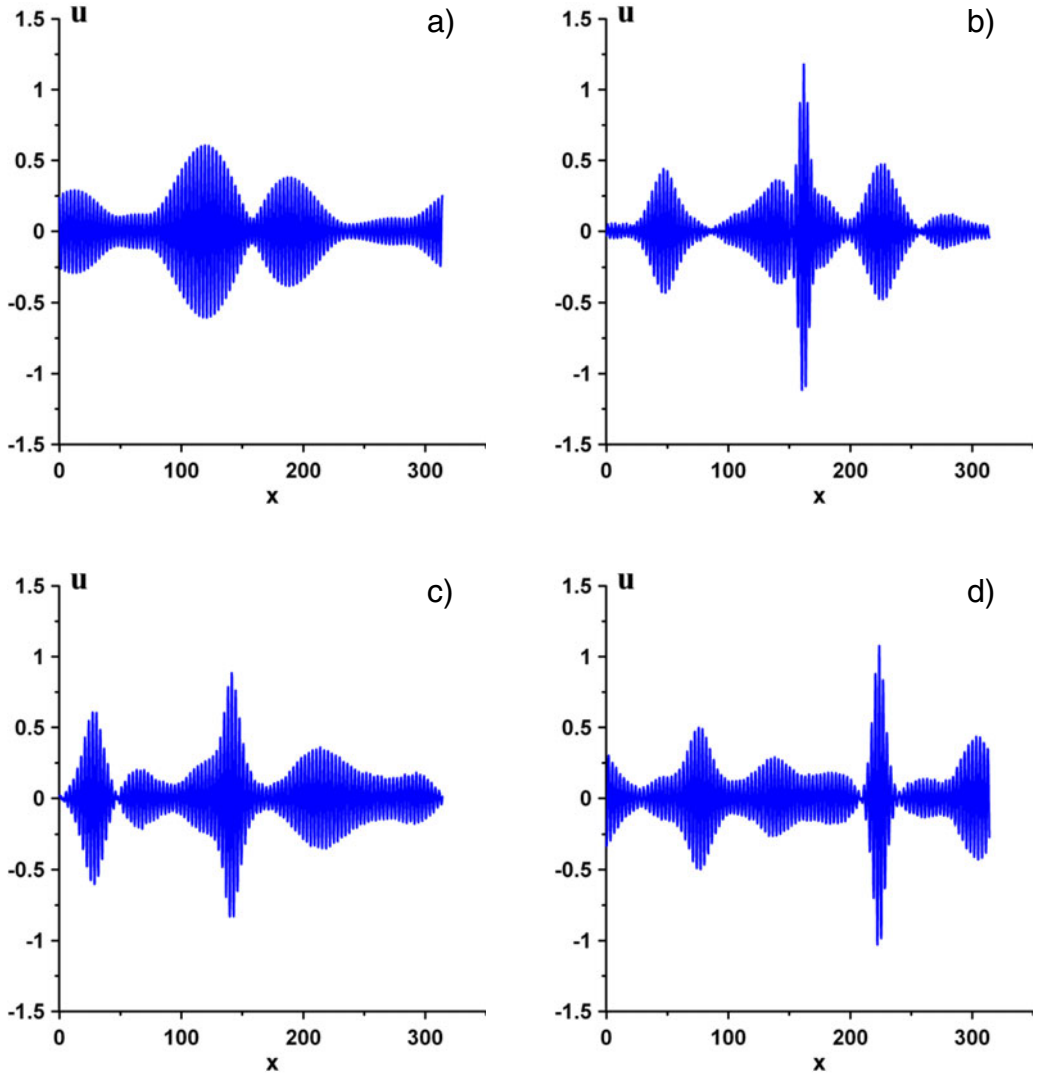

Fig. 4. Wave group evolution with initial amplitude 0.6, 6 satellites; (a) $t = 0$ top left, (b) $t = 50$ top right, (c) $t = 400$ bottom lefft, (d) $= 500$ bottom right.

spectrum does not satisfy Gaussian statistics, and indeed nonlinear energy focusing can still occur leading to the occurrence of some large waves.

Here we examine the possibility of rogue wave formation within the context of the Gardner equation, which is an extension of the KdV equation which contains both quadratic and cubic nonlinear terms. This model is commonly used to describe internal solitary waves in the coastal oceans. There are two versions of the Gardner equation, depending on the relative signs of the coefficients of the cubic nonlinear term and the linear dispersive term (see below). When these have the opposite sign, an asymptotic reduction leads to the defocusing NLS equation, and hence we expect that random wave fields would evolve in a manner qualitatively similar the KdV case. But when the coefficients have the same sign, wave packets with a sufficiently large carrier wavenumber are described by the focusing NLS equation, see Grimshaw et al. (2001), implying the possibility for the enhanced formation of rogue waves by modulational instability. Hence, this is the case of interest in this study, and we note that this version of the Gardner equation can arise in many parts of the coastal oceans, see Grimshaw et al. (2007). Further the Gardner equation has no direct analogy in the theory of the nonlinear surface waves.

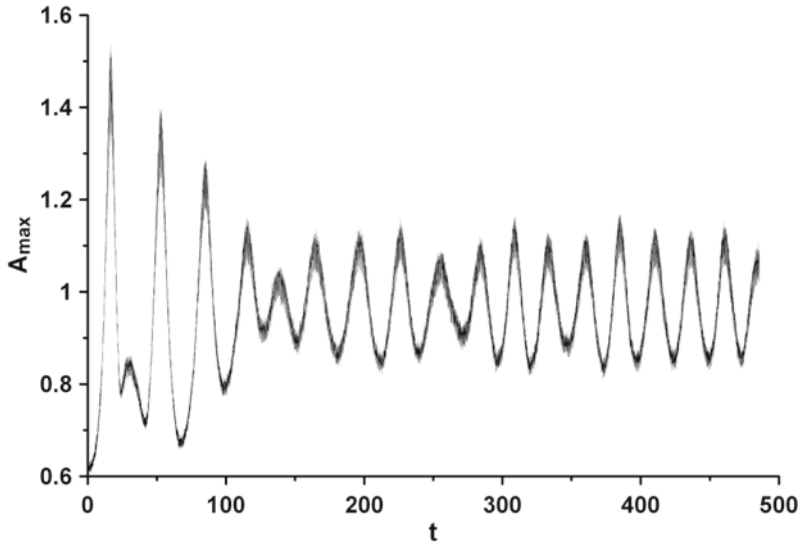

Fig. 5. Variations of the maximum amplitude with time for an initial maximum amplitude of 0.6, 6 satellites.

In Sect. 2 we give a brief description of the Gardner equation, and then in Sect. 3 we present our numerical results for the evolution of an initial narrow-band modulated wave field. We conclude in Sect. 4 with a discussion.

2 Gardner equation

The Gardner equation for the description of long nonlinear internal waves is

$$\eta_t + \alpha\eta\eta_x + \beta\eta^2\eta_x + \delta\eta_{xxx} = 0\,. \tag{1}$$

Here $\eta(x,t)$ is the amplitude of a linear long wave mode with phase speed c_0, and equation (1) has been written in a reference frame moving with speed c_0. The coefficients α, β, δ are determined by the background density stratification and the background horizontal current, see Grimshaw (2001), Holloway et al. (2001) or Grimshaw et al. (2007). Without loss of generality, we choose $c_0 > 0$ and then it can be shown that the dispersive coefficient $\delta > 0$. However, the nonlinear coefficients α, β can take either sign, and as above, we are concerned here with the case when $\beta > 0$. Without loss of generality, the Gardner equation (1) can then be transformed to the dimensionless form,

$$u_t + uu_x + u^2u_x + u_{xxx} = 0\,. \tag{2}$$

In the remainder of this paper, our analysis and numerical solutions are based on equation (2).

Our interest here is in wave groups, and hence for a weakly nonlinear waves, we seek an asymptotic reduction to a nonlinear Schrodinger equation. Thus we introduce an asymptotic expansion of the form

$$u = \epsilon A(X,\tau)\exp(ikx - i\omega(k)t) + \cdots + \text{c. c.}\,, \quad X = \epsilon(x - c_g t), \quad \tau = \epsilon^2 t\,. \tag{3}$$

Here c. c. denotes the complex conjugate, $\cdots$ denotes terms of $O(\epsilon^2)$ which include second harmonic and mean flow terms, and we have included the leading-order result that the wave envelope $A(X,T)$ will propagate with the group velocity $c_g = \partial\omega/\partial k$, where $\omega = \omega(k)$ is the linear dispersion relation. For the Gardner equation (2), $\omega(k) = -k^3$ and so $c_g = -3k^2$. A straight-forward but lengthy asymptotic analysis then yields the nonlinear Schrodinger equation (see Grimshaw et al., 2001)

$$iA_\tau = \lambda A_{XX} + \mu|A|^2A\,, \quad \lambda = 3k, \quad \mu = 1 - \frac{1}{6k^2}. \tag{4}$$

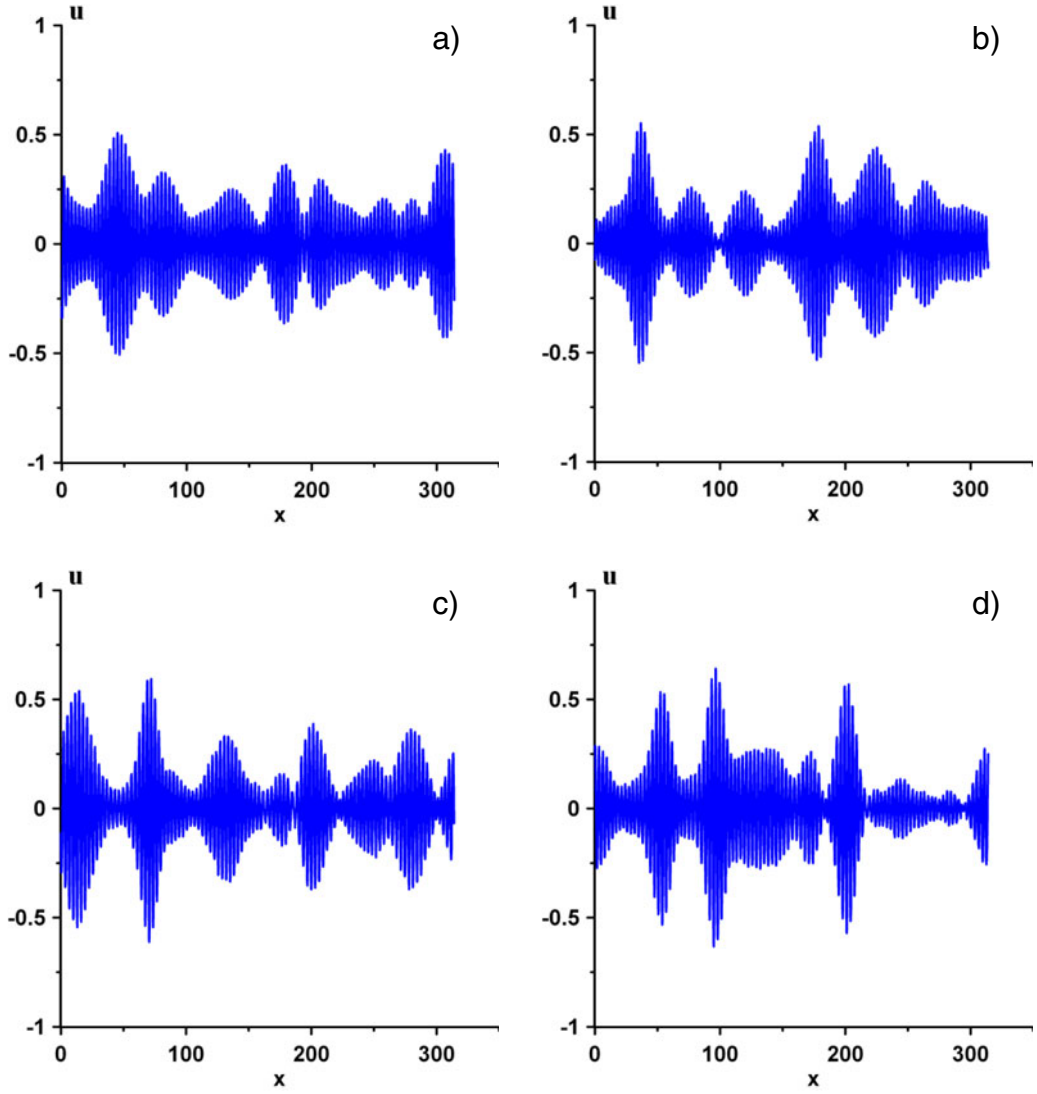

Fig. 6. Wave group evolution with initial amplitude 0.5, 20 satellites; (a) $t = 0$ top left, (b) $t = 200$ top right, (c) $t = 400$ bottom left, (d) $t = 500$ bottom right.

It now follows immediately that the wave packet (3) is modulationally unstable whenever the nonlinear Schrodinger equation is of the focusing kind, that is whenever $\lambda\mu > 0$. Hence we infer that for the Gardner equation (2) there is modulational instability when the carrier wave number satisfies the following condition (see Grimshaw et al., 2001)

$$k > \sqrt{\frac{1}{6}} \approx 0.41. \tag{5}$$

Further whenever condition (5) holds, modulational instability occurs with a modulation wavenumber K such that $K^2 < 2\mu|A_0|^2/\lambda$ with a maximum growth rate of $|\lambda A_0|^2$ when $K^2 = \mu|A_0|^2/\lambda$, where A_0 is the amplitude of the modulated plane wave. Numerical simulations by Grimshaw et al. (2001) demonstrated that the outcome of modulational instability is the generation of envelope solitary waves and breathers, which for small amplitude waves can be described by the nonlinear Schrodinger equation (4), and for larger amplitudes are associated with the breather solutions of the full Gardner equation (2). Such breathers can be obtained in

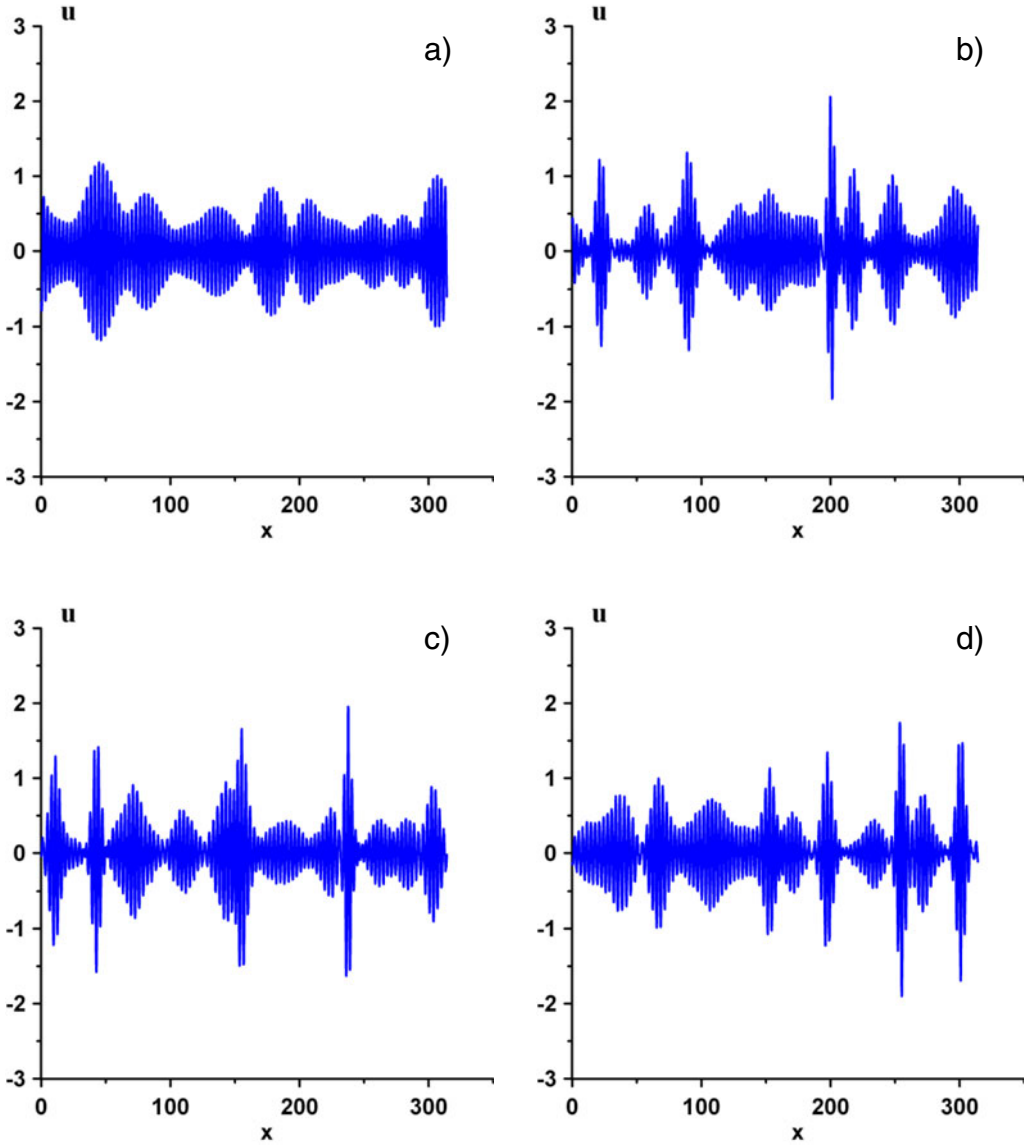

Fig. 7. Wave group evolution with initial amplitude 1.2, 20 satellites; (a) $t = 0$ top left, (b) $t = 150$ top right, (c) $t = 400$ bottom left, (d) $t = 500$ bottom right.

the full nonlinear Euler equation, see Lamb et al. (2007). In this paper we revisit this issue of modulational instability for the Gardner equation (2) and focus specifically on criteria which can lead to rogue wave formation.

3 Dynamics of modulated initial narrow-band wave field

The Gardner equation is solved by a finite-difference scheme which is described in Holloway et al. (1997, 1999), where the Courant criterion is satisfied by choosing the time step Δt as

$$\Delta t < 0.38(\Delta x)^3, \tag{6}$$

where Δx is the spatial step. Then Eq. (2) is solved with the periodic boundary condition

$$u(x + L, t) = u(x, t)\,, \tag{7}$$

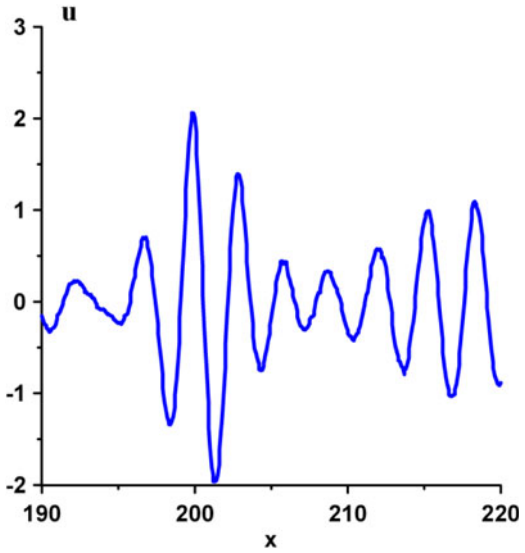

Fig. 8. Zoom of Fig. 7(b).

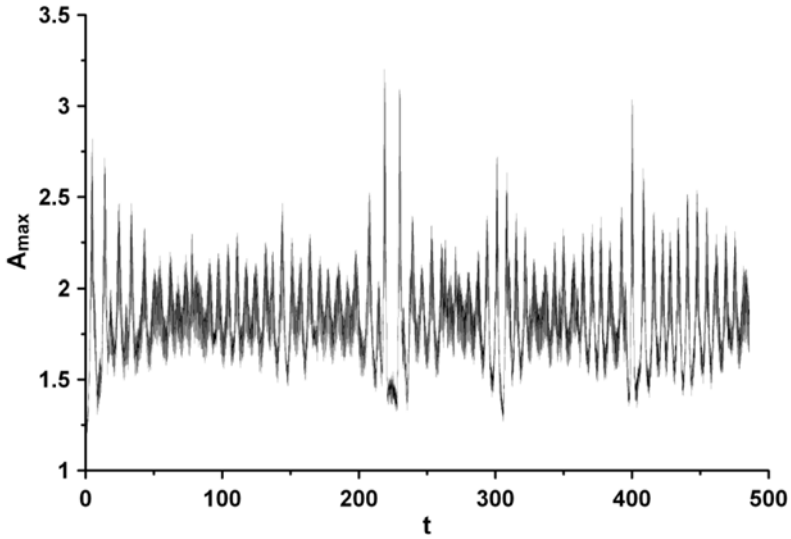

Fig. 9. Variations of the maximum amplitude with time for an initial maximum amplitude of 1.2, 20 satellites.

where L is the spatial domain length, and with the initial condition

$$u(x,0) = u_0(x)\,. \tag{8}$$

The mass and momentum conservation laws of the Gardner equation (2) are controlled in our numerical simulations.

We take the initial wave as a narrow-band Gaussian spectrum in the form

$$u(x,0) = \sum_{i=-N/2}^{N/2} a_i \cos\left(k_i x + \phi_i\right), \tag{9}$$

$$\text{where} \quad a_i = (2S_i)^{1/2}\,, \quad S_i = \exp(-k_i - k_0)^2/\Delta \mathrm{K}^2). \tag{10}$$

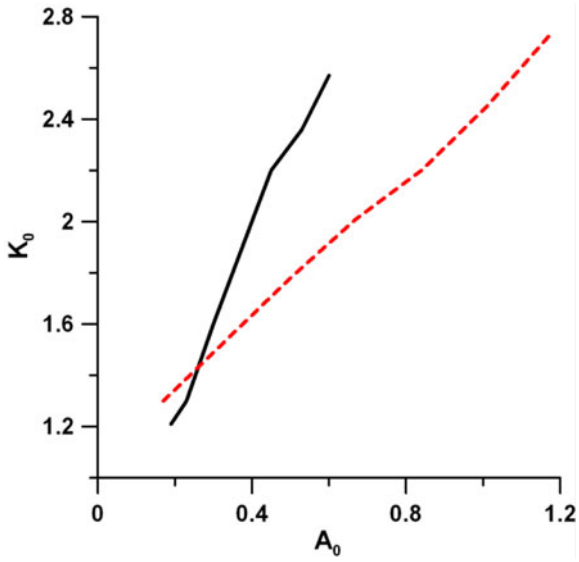

Fig. 10. Amplification factor K_0 versus the initial maximum amplitude A. The black line is for six satellites and the red line is for twenty satellites.

$\Delta K = 0.1$ is the width of the spectrum, and ϕ_i are arbitrary phases chosen by a random number generator. The carrier wave number $k_0 = 2$ in our numerical experiments. We take 6 ($N = 6$) and 20 ($N = 20$) satellite harmonics symmetrically placed about the carrier wave number k_0, with a step of 0.02 between neighbours. The total computational time is 500. Note that from the discussion of the modulational instability in Sect. 2, we infer that a suitable nonlinear time scale is proportional to $1/\lambda|A_0|^2$. With $\lambda = 3k_0 = 6$ and with amplitudes $2A_0 = 2A(X, 0)$, see (3), typically greater than 0.1, our computational time is much greater than the time scale for modulational instability.

3.1 Six satellites

The initial wave field contains three modulated groups, see Fig. 3(a) ($A_{max} = 0.23$). The nonlinear evolution of the wave field is displayed in Fig. 3. In the first stage the amplitude of central group grows (approximately by a factor 1.3), its shape is symmetric and it looks like a breather (Fig. 3(b)). Then the amplitudes of all the groups become comparable, they merge and their shapes become asymmetrical (Figs. 3(c), (d)). Qualitatively, the wave dynamics is similar to the evolution of wave packets in the framework of the modified Korteweg-de Vries equation and the nonlinear Schrodinger equation (Grimshaw et al., 2001, 2005). Due to the weak initial wave amplitude there is no the rogue waves formation.

With an increase in the initial wave amplitude ($A_{max} = 0.6$), the amplification can be more than twice and reaches 2.6 (Fig. 4). The wave packet of maximal amplitude is narrower, and contains only 5–7 individual waves. Rogue waves are formed several times as is illustrated in Figs. 4(b), (d). A more detailed analysis of the maximal wave amplitude variation versus time is shown in Fig. 5. First, the maximum amplitude begins from the initial value 0.6 and never returns to this value. The oscillations in amplitude are largest for small times (reaching 1.55) and tend to quasi-periodic variations about a mean value (approximately 1) with a deviation of 0.2. The maximum amplification factor here is about 2.6. The following maximum of 1.38 after this is reached at about the time moment 50 (the wave field for this time is displayed on Fig. 4(b)) and amplification factor here is only 2.3. The third maximum in the wave amplitude (1.3) is reached at about the time moment 85, and the amplification factor here is about 2. Thus, three rogue waves can be selected here. In fact, all waves with amplitudes exceeding 1 could be considered as rogue waves if their amplitudes are compared with the mean wave amplitude.

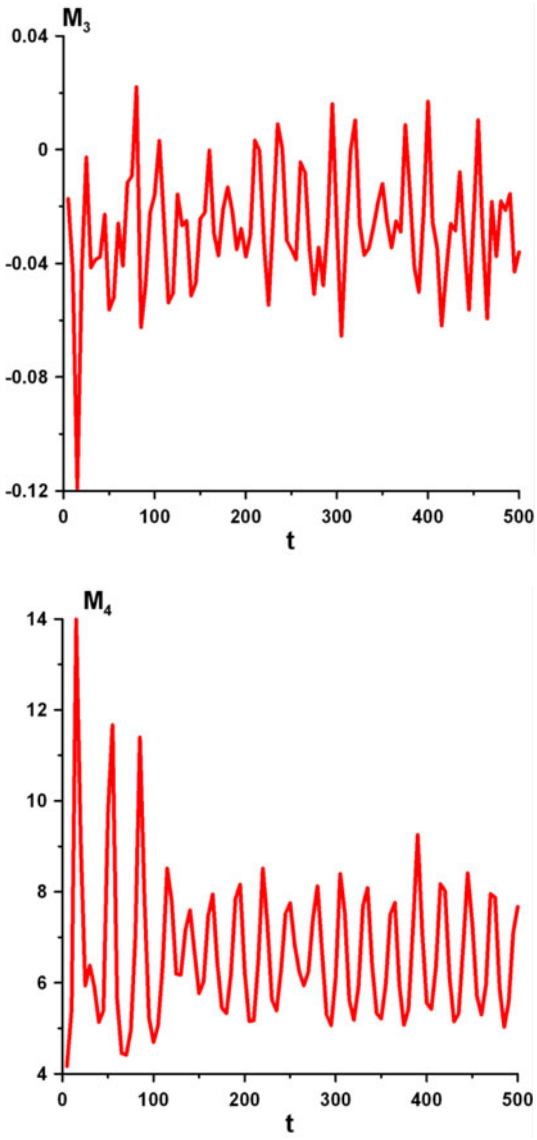

Fig. 11. Third (top panel) and fourth (bottom panel) moments of the wave field with $A_{max} = 0.6$ (six satellites).

Qualitatively, the wave dynamics is similar to that in the modified Korteweg-de Vries equation and nonlinear Schrodinger equation (Grimshaw et al., 2001, 2005). There is no visible asymmetry with respect to the horizontal axis, as can be expected in the framework of the Gardner equation. Also, the periodicity in the maximal wave amplitude (Fig. 5) can be related with recurrence phenomenon in the nonlinear Schrodinger equation.

3.2 Twenty satellites

Twenty satellites just fulfills the condition for a narrow initial spectrum. The evolution of the wave field with $A_{max} = 0.5$ is displayed in Fig. 6. Now, the initial wave field consists to eight modulated groups of different amplitudes and each group contains 9–15 individual waves. Breather-like groups with some larger amplitudes than the initial one form with time (Figs. 6(c), (d)). The maximum amplification factor here is 1.3. Qualitatively, the wave dynamics are the same as in models based on the nonlinear Schrodinger equation.

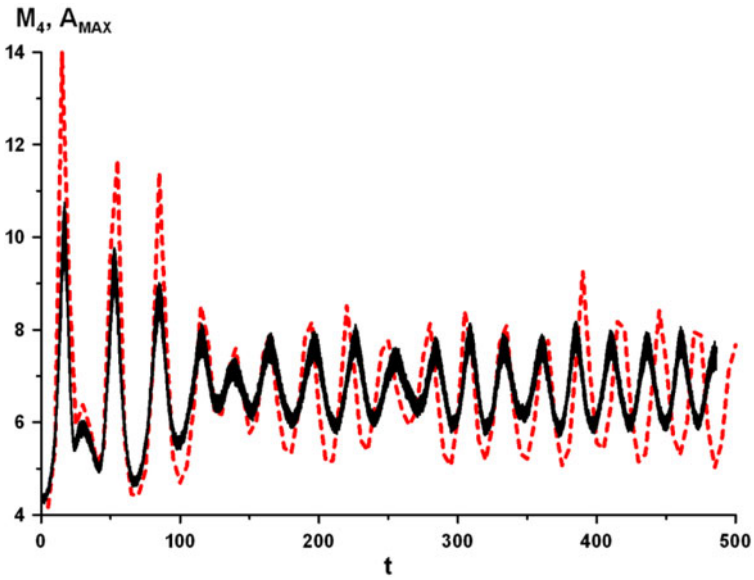

Fig. 12. Fourth moment (red and dash) and maximum amplitude (black and solid) (multiplied by 7) for the wave field with $A_{max} = 0.6$ (six satellites).

An increase of the initial amplitude leads to more complicated wave dynamics. The wave field with $A_{max} = 1.2$ is shown on Fig. 7 for various times. The breathers formed here are narrower than in the previous case (3–5 individual waves). The largest waves here are two individual waves, and are not a wave group (Fig. 8).

The maximum amplitude versus time for this case is shown in Fig. 9. The curve looks more chaotic and large amplitude waves appear many times. The biggest maximum here (3.24) is not the first one and it is reached at time 220 (the maximum amplification factor is about 2.74). Amplitudes more than 2.4 (twice more than the initial largest one of amplitude 1.2) are reached about 14 times over the computational time.

3.3 Comparison for different satellite numbers

A comparison of the computed values of the amplification factor K_0 (the ratio of the maximum wave amplitude over the computational time to the maximum initial amplitude) for various numbers of satellites is given in Fig. 10. We see that an increase in the spectral width leads to a reduction in the amplification factor. Indeed this conclusion is known for modulational instability in the framework of nonlinear Schrodinger equation (Alber, 1978) and is here confirmed in the framework of the Gardner equation.

Additionally, several integrals of the wave field are computed. As indicated above, the mass ($M_1 = \int u dx$) and momentum ($M_2 = \int u^2 dx$) integrals are conserved for the Gardner equation (2). The third and fourth integrals (moments)

$$M_3(t) = \frac{\int u^3 dx}{(\int u^2 dx)^{3/2}}, \quad M_4(t) = \frac{\int u^4 dx}{(\int u^2 dx)^2}, \tag{11}$$

characterize in statistical theory (after averaging an ensemble of realizations) the skewness and kurtosis (deviation from a Gaussian distribution where $M_3 = 0$, $M_4 = 3$). Here they are computed for only one realization of the wave field and hence vary in time. Although the wave field modeled here by a finite number of harmonics can not be strictly Gaussian (since the conditions for the central limit theorem are not satisfied), nevertheless the variation of these moments with time can demonstrate a tendency in nonlinear wave interactions. In particular, the behavior for six satellites is illustrated on Fig. 11. The third moment (skewness) is mainly negative which implies that waves of negative polarity dominate in the wave field. It starts from

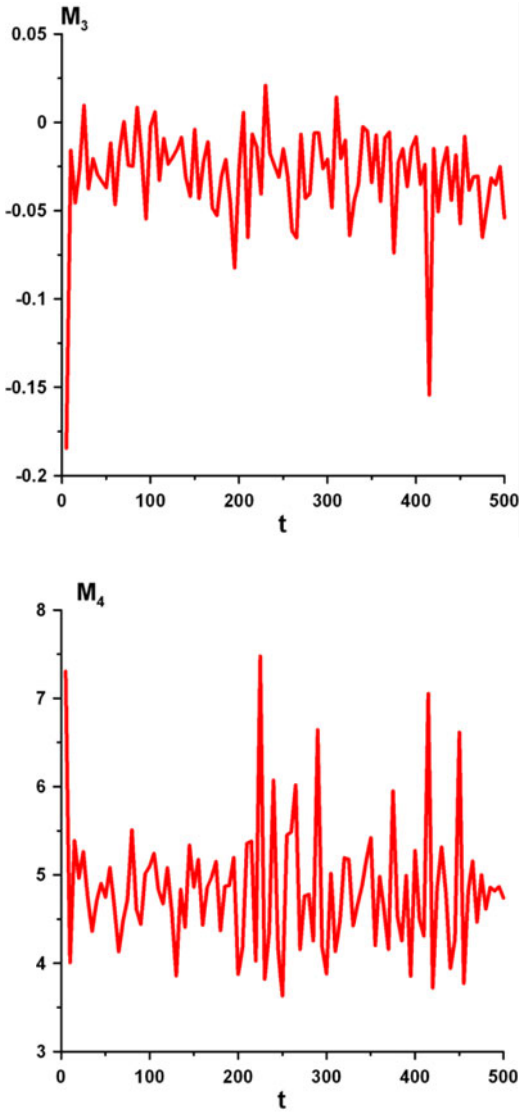

Fig. 13. Third (top panel) and fourth (bottom panel) moments of the wave field with $A_{max} = 1.2$ (twenty satellites).

a value close to zero (-0.02) and reaches a minimum value -0.12 after a short time. Then it oscillates around a mean value of about -0.02. The fourth moment (kurtosis) is positive and starts from 4 to reach a first maximum of 14. Then it reaches its second and third maximum of 11.7 and 11.4 after which it oscillates around a mean value 6.7. As is well-known a Gaussian wave field has a kurtosis of 3, and thus the probability of the appearance of large-amplitude waves (rogue waves) is higher then for a linear wave field. It is interesting to point out that the behavior of the fourth moment is well correlated with the behavior of the maximum amplitude (Fig. 12) confirming the contribution of large-amplitude waves to the kurtosis.

In the case of twenty satellites the time evolution of the third and the fourth moments is shown in Fig. 13. The first minimum in the third moment is reached at a time 5 and equals -0.18. After that the third moment oscillates around -0.025 and is mainly negative. The second minimum -0.15 is reached at a time 415. Increasing the number of satellites leads to a decrease of the deviation of the skewness from the mean value as is expected in statistical averaging. The fourth moment (kurtosis) exceeds 3 and reaches a first maximum of 7.3 at time 5, after which it oscillates with an amplitude less than 1 around the mean value 4.8 to a time

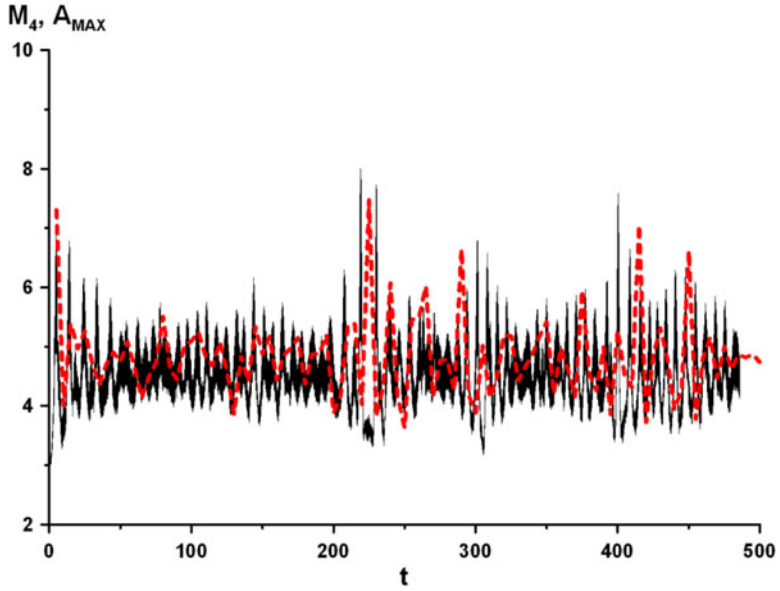

Fig. 14. Fourth moment (red and dash) and maximum amplitude (black and solid) (multiplied by 2.5) for the wave field with $A_{max} = 1.2$ (twenty satellites).

230. Beyond this time we see four maximum lying between 6.8 and 7.5. Again the kurtosis on average correlates with the maximum wave amplitude (Fig. 14), but the oscillations in the maximum amplitude are more frequent than in the fourth moment.

4 Discussion

In this paper we have reported numerical simulations of the Gardner equation (2) when the initial condition is a modulated narrow-band wave field. Our initial conditions are chosen to lie in the regime of modulational instability for a plane wave, and hence it is no surprise that we find the emergence of rogue waves. More explicitly, we see the occurrence of spatially and temporally localized large waves, typically more than twice the background waves.

In the Introduction we motivated this study by the fact that the Gardner equation is commonly used to model internal waves in the coastal ocean. Hence we can infer that the results reported here suggest that under certain conditions rogue internal waves can arise in the coastal ocean. The first condition is that the background density stratification should be such that the relevant Gardner equation is that which has a positive coefficient of the cubic nonlinear term. This excludes the commonly-used two layer density stratification models, but does arise when the density stratification is modeled by three layers with a deep middle layer. Further the case of a positive cubic coefficient is relatively commonly found in the coastal oceans. Moreover, for the case of the Gardner equation with a negative coefficient of the cubic nonlinear term, when modulational instability is not allowed, we would expect that the evolution from an initial condition of a modulated narrow-band wave field would be similar to that reported for the KdV equation, where nonlinear energy focussing can still lead to the occurrence of large waves, see Pelinovsky and Sergeeva (2006).

Within the context of this present study, another condition for the occurrence of rogue internal waves is the initial presence of a narrow-band internal wave field. In most scenarios for the generation of internal solitary waves in the coastal ocean, the observed waves have instead the structure of a deterministic amplitude-ordered wavetrain, sometimes described as an internal undular bore. Our present results do not directly address the issue of whether rogue internal waves could eventually emerge from such an internal undular bore. But we can suggest that based on the results described here, this is certainly a possibility, especially if the amplitude ordering of the wavetrain was broken, say by the action of variable topography or the effects

of the earth's rotation, see for instance, Helfrich and Grimshaw (2007), Grimshaw and Helfrich (2008), Sanchez-Garrido and Vlasenko (2009) and Vlasenko et al. (2009).

Finally, as mentioned in the Introduction, there are several other mechanisms that have been proposed for rogue waves. Importantly, in the context of internal waves these include the essentially linear mechanisms of focussing of wave energy by topography or currents. Given the environmental variability of the coastal ocean, these are also likely to be important factors for the possible presence of rogue internal waves, and we emphasize that we have not considered them at all in this paper. Nevertheless, although the numerical simulations of the Gardner equation that we have reported here have a limited context, they do provide evidence that internal rogue waves in the coastal ocean are a real possibility.

Grants RFBR (08-05-00069, 09-05-91850, 09-05-00204, 09-05-90408) are acknowledged.

References

1. N. Akhmediev, J.M. Soto-Crespo, A. Ankiewicz, Phys. Rev. A **80**, 043818 (2009)
2. I.E. Alber, Proc. Roy. Soc. London **A363**, 525 (1978)
3. J.R. Apel, L.A. Ostrovsky, Y.A. Stepanyants, J.F. Lynch, J. Acoust. Soc. Am. **121**, 695 (2007)
4. P. Caillol, V. Zeitlin, Dynamics Atmos. Oceans **33**, 325 (2001)
5. T.F. Duda, J.F. Lynch, J.D. Irish, R.C. Beardsley, S.R. Ramp, et al., IEEE J. Ocean. Eng. **29**, 110531 (2004)
6. R. Grimshaw, Internal solitary waves, in *Environmental Stratified Flows*, edited by R. Grimshaw, Chapter 1 (Kluwer Acad. Publ., 2001), p. 1
7. R. Grimshaw, D. Pelinovsky, E. Pelinovsky, T. Talipova, Physica D **159**, 35 (2001)
8. R. Grimshaw, E. Pelinovsky, T. Talipova, M. Ruderman, R. Erdely, Stud. Appl. Math. **114**, 189 (2005)
9. R. Grimshaw, E Pelinovsky, T. Talipova, Surveys Geophys. **28**, 273 (2007)
10. R. Grimshaw, K.R. Helfrich, Stud. Appl. Math. **121**, 71 (2008)
11. K.R. Helfrich, R.H.J. Grimshaw, J. Phys. Ocean. **38**, 686 (2008)
12. P. Holloway, E. Pelinovsky, T. Talipova, B. Barnes, J. Phys. Ocean. **27**, 871 (1997)
13. P. Holloway, E. Pelinovsky, T. Talipova, J. Geophys. Res. **104**, 18333 (1999)
14. P. Holloway, E. Pelinovsky, T. Talipova, in *Environmental Stratified Flows*, edited by R. Grimshaw Chapter 2 (Kluwer Acad. Publ., 2001), p. 29
15. C. Kharif, E. Pelinovsky, A. Slunyaev, Adv. Geophys. Env. Mech. Math. **14**, 216 (2009)
16. K. Lamb, O. Polukhina, T. Talipova, E. Pelinovsky, W. Xiao, A. Kurkin, Physical Rev. E **75**, 046306 (2007)
17. A.K. Liu, Y.S. Chang, M.-K. Hsu, N.K. Liang, J. Geophy. Res. **103**, 7995 (1998)
18. A.K. Liu, S.R. Ramp, Y. Zhao, T.Y. Tang, IEEE J. Ocean. Eng. **29**, 144 (2004)
19. Ch.-T. Liu, R. Pinkel, J. Klymak, M.-K. Hsu, H.-W. Chen, C. Villanoy, EOS **87**, 449451 (2006)
20. Y.V. Lvov, K.L. Polzin, E. Tabak, Phys. Rev. Lett. **92**, 128501 (2004)
21. C.H. McMomas, J. Phys. Ocean. **7**, 836 (1977)
22. P. Muller, D.J. Olbers, J. Geophys. Res. **80**, 3848 (1975)
23. D.J. Olbers, J. Fluid Mech. **74**, 375 (1976)
24. M.H. Orr, P.C. Mignerey J. Geophy. Res. **108**, 3064 (2003)
25. E. Pelinovsky, M.A. Raevsky, Izvestiya Atmos. Ocean. Physics **13**, 130 (1977)
26. E. Pelinovksy, A. Sergeeva, Eur. J. Mech. B/Fluids **25**, 425 (2006)
27. J.C. Sanchez-Garrido, Vlasenko V. V., Nonlin. Processes Geophys. **16**, 587598 (2009)
28. D.R. Solli, C. Ropers, P. Koppnath, B. Jalali, Nature **450**, 1054 (2007)
29. V. Vlasenko, N. Stashchuk, J. Geophys. Res. **112**, C11018 (2007)
30. V. Vlasenko J.C. Sanchez-Garrido, N. Stashchuk, J.G. Lafuente, M. Losada, J. Phys. Ocean. **39**, 2230 (2009)
31. A.C. Warn-Varnas, S.A. Chin-Bing, D.B. King, J.A. Hawkins, K.G. Lamb, M. Teixeira, J. Geophys. Res. **110**, C08001 (2005)
32. D.-ll. Yeom, B.J. Eggleton, Nature **450**, 953 (2007)